Magnetic ordering and Kondo behavior in single-crystalline Ce_2NiSi_3

Maria Szlawska and Dariusz Kaczorowski

Institute of Low Temperature and Structure Research, Polish Academy of Sciences, P. O. Box 1410, 50-950 Wrocław, Poland

(Received 17 October 2011; revised manuscript received 20 March 2012; published 13 April 2012)

A single crystal of Ce_2NiSi_3 was studied by means of x-ray-diffraction, magnetization, heat-capacity, and electrical resistivity measurements, performed in the temperature range 0.4–300 K and in magnetic fields up to 9 T. The compound was found to crystallize with a disordered AlB_2-type structure. Ce_2NiSi_3 orders antiferromagnetically below $T_N = 3.2$ K, as inferred from distinct anomalies in the magnetic susceptibility, heat-capacity, and electrical resistivity data. Large, negative values of the paramagnetic Curie temperature, enhanced electronic contribution to the specific heat, and logarithmic slopes in the electrical resistivity hint at the presence of Kondo interactions.

DOI: 10.1103/PhysRevB.85.134423 PACS number(s): 75.50.Ee, 71.27.+a, 75.30.Mb

I. INTRODUCTION

Ternary intermetallics with the overall composition R_2TM_3, where R is a rare-earth or uranium atom, T stands for a d-electron transition metal, and M is a p-electron element, commonly crystallize with a simple hexagonal AlB_2-type unit cell or its more or less ordered derivatives.[1] These phases exhibit a large variety of magnetic characteristics, which are related to their crystal structures. The compounds in which T and M atoms share a single crystallographic position usually show spin-glass-like behavior, as observed for example in Ce_2CuGe_3,[2] Ce_2AgIn_3,[3] and the U-based phases U_2TSi_3 for T = Co, Ni, Rh, Pd, Ir, Pt, and Au.[4–12] In contrast, structurally ordered R_2TM_3 phases often exhibit long-range magnetic ordering, as found, e.g., for the phases RE_2RhSi_2 for RE = Ce, Nd, Sm, Gd, Tb, Dy, Ho, and Er,[13–17] or remain paramagnetic down to very low temperatures, as is the case, e.g., for Ce_2CoSi_3[18–20] and the compounds U_2TSi_3 with T = Fe and Ru.[5,21]

The Ce-based phases Ce_2NiM_3 with M = Si, Ge, and In crystallize with the AlB_2-type structure.[22] Two of them, namely, Ce_2NiGe_3 and Ce_2NiIn_3, have been characterized as spin glasses with the freezing temperature of 3.5 and 2.8 K, respectively.[23,24] In contrast, in Ce_2NiSi_3 an antiferromagnetic ground state has been revealed by means of magnetic susceptibility and heat-capacity measurements of polycrystalline samples,[25,26] which seemed fairly unexpected for a R_2TM_3 compound with a strongly disordered unit cell. However, specimens prepared in different laboratories showed somewhat divergent bulk characteristics,[18,25,26] and the Néel temperature appeared notably dependent on postcast thermal treatment of polycrystalline material.[26] The present study aimed at clarifying the intrinsic magnetic properties of Ce_2NiSi_3 by means of detailed measurements of high-quality single crystals, performed in wide ranges of temperature and magnetic-field strengths.

II. EXPERIMENTAL DETAILS

A single crystal of Ce_2NiSi_3 was grown by the Czochralski pulling method using a tetra-arc furnace. The starting components were high-purity elements (Ce-3N, Ni-5N, and Si-6N). The obtained crystal was 5 mm in diameter and 15 mm in length. The specimens for x-ray analysis and for physical properties measurements were cut from the single-crystalline rod using a high-precision wire saw.

The single-crystal x-ray-diffraction data were collected on an Oxford Diffraction four-circle diffractometer equipped with a charge coupled device camera using Mo Kα radiation. Crystal structure refinement was performed employing the program SHELXL-97.[27] Details on the single-crystal data collection and the structure refinement are given in Table I.

A polycrystalline sample of La_2NiSi_3, used as a nonmagnetic counterpart to the cerium compound studied, was synthesized by arc melting the stoichiometric amounts of the elemental components (La-3N, Ni-5N, and Si-6N) under a Ti-gettered argon atmosphere. The button was flipped over and remelted several times to ensure good homogeneity. Quality of the so-obtained material was checked by x-ray diffraction on a Stoe powder diffractometer with Cu Kα radiation and by energy dispersive x-ray analysis using a Phillips 515 scanning electron microscope equipped with an EDAX PV 9800 probe. The structure refinement was done employing the program FULLPROF.[28]

Magnetic measurements were performed within the temperature range 1.72–400 K and in magnetic fields up to 5 T using a Quantum Design MPMS-5 superconducting quantum interference device magnetometer. The heat capacity was measured in the temperature interval 0.5–300 K and in magnetic fields up to 9 T, using a Quantum Design PPMS-9 platform. The temperature and magnetic-field variations of the electrical resistivity were studied from 0.5 to 300 K and in magnetic fields up to 9 T, applied perpendicular to the a.c. current flowing through the specimen. For these measurements a Quantum Design PPMS-9 platform was employed.

III. RESULTS AND DISCUSSION

A. Crystal structure

The crystal structure refinement of the single-crystal x-ray-diffraction data of Ce_2NiSi_3 corroborated the previous findings of the hexagonal AlB_2-type unit cell,[18,25,26] in which the Ce atoms occupy the Al 1a position, while the Ni and Si atoms share the unique B 2d site. The crystal structure (shown in Fig. 1) consists of alternating layers of the Ce and Ni/Si atoms, stacked along the c axis. The Ce atoms are arranged into primitive hexagonal arrays that form trigonal prisms, inside

TABLE I. Crystallographic and structure refinement data for Ce_2NiSi_3.

Compound	Ce_2NiSi_3
Space group	$p6/mmm$
Unit-cell dimensions	$a = 4.0450(6)$ Å
	$c = 4.2830(9)$ Å
Volume	60.690(18) Å^3
Formula weight	423.18 g/mol
Calculated density	5.790 g/cm^3
Absorption coefficient	22.821 mm^{-1}
θ range for data collection	4.76–47.06°
Ranges in hkl	$-6 \leqslant h \leqslant 8$
	$-8 \leqslant k \leqslant 4$
	$-7 \leqslant l \leqslant 5$
Reflections collected/unique	1352/134 [R(int) = 0.0666]
Completeness to $\theta = 47.06$°	90.05%
Refinement method	Full-matrix least squares on F^2
Data/restrains/parameters	134/0/7
Goodness of fit on F^2	1.091
Final R indices [$I \geqslant 2\sigma(I)$]	$R1 = 0.0204$, $wR2 = 0.0372$
R indices (all data)	$R1 = 0.0204$, $wR2 = 0.0372$
Extinction coefficient	0.023(2)
Largest diff. peak and hole	2.028 and −1.567 e/Å^{-3}

which the nonmagnetic atoms are randomly distributed. The atomic coordinates, the thermal displacement parameters, and the principal interatomic distances are given in Tables II–IV, respectively.

The x-ray powder-diffraction experiment revealed that La_2NiSi_3 is isostructural to its Ce-based counterpart. The refined hexagonal lattice parameters $a = 4.0689(3)$ Å and $c = 4.3753(4)$ Å are in good agreement with those reported in the literature.[26]

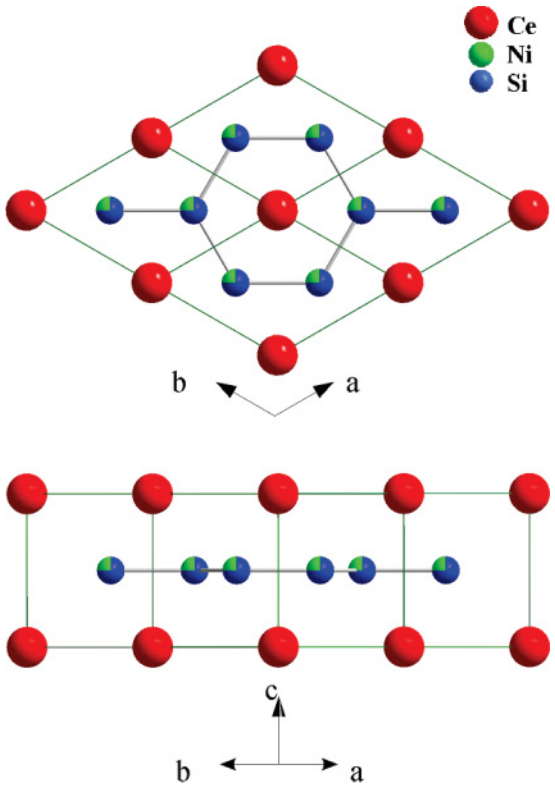

FIG. 1. (Color online) Crystal structure of Ce_2NiSi_3.

TABLE II. Site coordinates and equivalent isotropic thermal displacement parameters (in Å$^2 \times 10^3$) for the atoms in the Ce_2NiSi_3 unit cell. U_{eq} is defined as one third of the trace of the orthogonalized U_{ij} tensor.

Atom	Site	x	y	z	U(Eq.)
Ce	1a	0	0	0	11(1)
Ni	2d	2/3	1/3	1/2	12(1)
Si	2d	2/3	1/3	1/2	12(1)

B. Magnetic properties

Figure 2 shows the temperature dependence of the inverse molar magnetic susceptibility of single-crystalline Ce_2NiSi_3, measured parallel and perpendicular to the hexagonal c axis. Above about 100 K, both components follow the Curie-Weiss (CW) law $\chi = \frac{\mu_{\rm eff}^2}{8(T-\theta_P)}$ with the least-square-fitting parameters $\mu_{\rm eff}^{\perp} = 2.56\ \mu_B$ and $\theta_P^{\perp} = -10$ for $B \perp c$ and $\mu_{\rm eff}^{\parallel} = 2.67\ \mu_B$ and $\theta_P^{\parallel} = -136$ K for $B \parallel c$. The obtained values of $\mu_{\rm eff}$ are fairly close to the effective magnetic moment predicted within the Russell-Saunders coupling scenario for trivalent cerium ions [$g\sqrt{j(j+1)} = 2.54$]. For both magnetic-field directions, yet especially for $B \parallel c$, the paramagnetic Curie temperature is strongly negative, which may result from either f-ligand hybridization or crystalline electric-field effects. The latter seems to be responsible for the large difference between values of θ_p taken along the crystallographic a and c axes, reflecting strong magnetocrystalline anisotropy in the compound. Below about 100 K, the magnetic susceptibility of Ce_2NiSi_3, particulary the component taken along the c axis, considerably deviates from the CW behavior due to gradual depopulation of excited crystalline electric-field levels.

The inset to Fig. 2 shows the low-temperature magnetic susceptibility, measured in a weak magnetic field of 0.01 T upon cooling the specimen in a zero (ZFC mode) and applied (FC mode) magnetic field. The plot reveals strong magnetic anisotropy with the component measured along the hexagonal c axis being much smaller than that taken within the a-b plane. For the latter field configuration, the $\chi_{\rm ZFC}(T)$ curve shows a clear maximum at 3.2 K, which manifests the onset of the antiferromagnetic ordering reported before.[25,26] However, the low-temperature $\chi_{\rm FC}(T)$ curve bifurcates from the ZFC data and forms a plateau below T_N. This finding implies the presence of a small ferromagnetic component

TABLE III. Anisotropic thermal displacement parameters for the atoms in the Ce_2NiSi_3 unit cell (in Å$^2 \times 10^3$). The anisotropic temperature factor exponent takes the form $-2\pi^2[h^2a^{*2}U_{11} + \cdots + 2hka^*b^*U_{12}]$.

Atom	$U11$	$U22$	$U33$	$U23$	$U13$	$U12$
Ce	11(1)	11(1)	10(1)	0	0	6(1)
Ni	11(1)	11(1)	13(1)	0	0	5(1)
Si	11(1)	11(1)	13(1)	0	0	5(1)

TABLE IV. Interatomic distances in the Ce_2NiSi_3 unit cell (in Å).

Ce	6 Ce	4.0450(6)
	2 Ce	4.2830(9)
	12 Ni/Si	3.1686(4)
Ni/Si	6 Ce	3.1686(4)
	3 Ni/Si	2.3354(4)

in the magnetic structure that has not been found in the previous studies.[25,26] With increasing magnetic-field strength, the difference between $\chi_{ZFC}(T)$ and $\chi_{FC}(T)$ rapidly decreases and becomes hardly observed in fields stronger than 0.3 T (see Fig. 3). Simultaneously, the maximum in $\chi_{ZFC}(T)$ disappears in a manner characteristic of metamagneticlike transitions. A metamagnetic anomaly near 0.8 T at $T = 2$ K has previously been observed for the annealed polycrystalline sample of Ce_2NiSi_3,[26] which showed however a distinctly higher Néel temperature $T_N = 4.2$ K and an additional magnetic transition at 2.5 K. In contrast, no metamagnetic features have been found for the as-cast polycrystal with $T_N = 3.8$ K,[26] which is closer to the critical temperature determined for the unannealed single crystal studied in the present work.

Figure 4 shows the field dependencies of the magnetization in single-crystalline Ce_2NiSi_3, measured along the two principal directions at 1.72 K, i.e., deeply in the ordered state. Both variations are in line with the antiferromagnetic type of the ordering, and the distinct magnetic anisotropy hints at the magnetic moments being mainly confined in the hexagonal a-b plane. A small remanence noticed in the magnetization taken with the $B \perp c$ axis (not shown) complies with the presence of a tiny ferromagnetic component in the nominally antiferromagnetic arrangement of the cerium magnetic moments. In turn, the metamagnetic transition evidenced in the magnetic susceptibility data finds no clear support in the magnetization

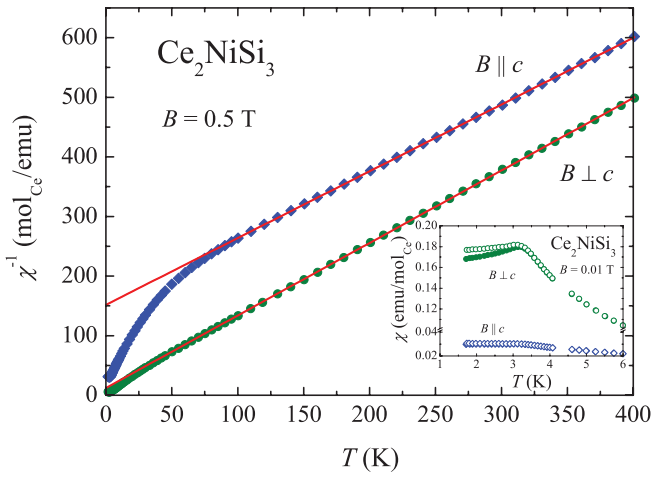

FIG. 2. (Color online) Temperature dependencies of the reciprocal molar magnetic susceptibility of single-crystalline Ce_2NiSi_3 measured with a magnetic field of 0.5 T oriented parallel and perpendicular to the c axis of the hexagonal unit cell. The solid lines represent the least-squares Curie-Weiss fits to the experimental data above 100 K. The inset shows the low-temperature magnetic susceptibility data, taken in a field of 0.01 T in the ZFC (full symbols) and FC (open symbols) modes.

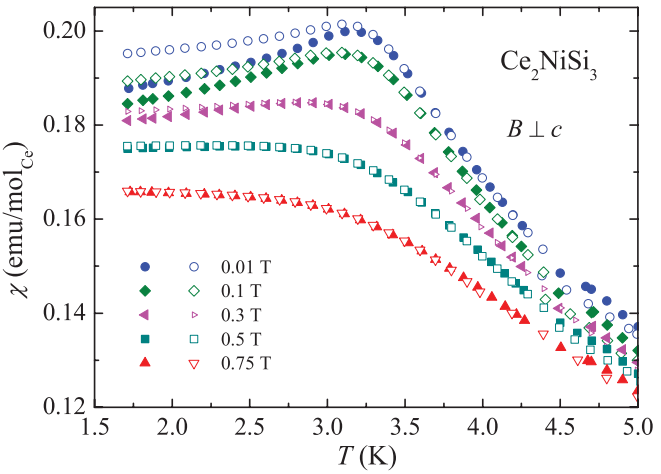

FIG. 3. (Color online) Low-temperature dependencies of the magnetic susceptibility of single-crystalline Ce_2NiSi_3, taken in three different magnetic fields oriented perpendicular to the hexagonal c axis. The full and open symbols represent the ZFC and FC data, respectively.

curves; namely, neither $\sigma(B)$ nor its field derivative exhibit any singularity at the critical field $B < 0.7$ T.

In contrast to the Ce-based compound, La_2NiSi_3 is a Pauli paramagnet, characterized by a hardly temperature-dependent magnetic susceptibility of the order of 10^{-4} emu/mol (not shown).

C. Heat capacity

Figure 5 presents the temperature dependence of the specific heat of Ce_2NiSi_3. At room temperature its magnitude approaches the Dulong-Petit limit, i.e., $C = 3nR = 149.58\ \mathrm{J\,mol^{-1}K^{-1}}$, where n is the number of atoms per molecule and R is the gas constant. At low temperatures (see the inset to Fig. 5), the specific heat is dominated by

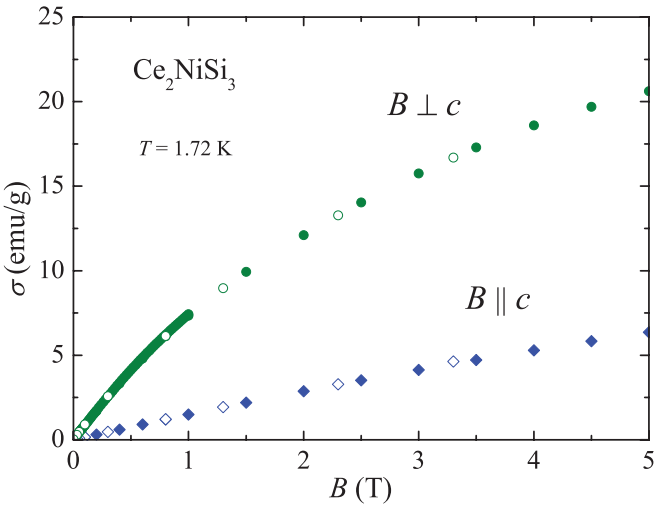

FIG. 4. (Color online) Magnetic-field variations of the magnetization in single-crystalline Ce_2NiSi_3 measured at a fixed temperature of 1.72 K with the magnetic field applied along and perpendicular to the hexagonal c axis. The full and open symbols represent the data obtained with increasing and decreasing field, respectively.

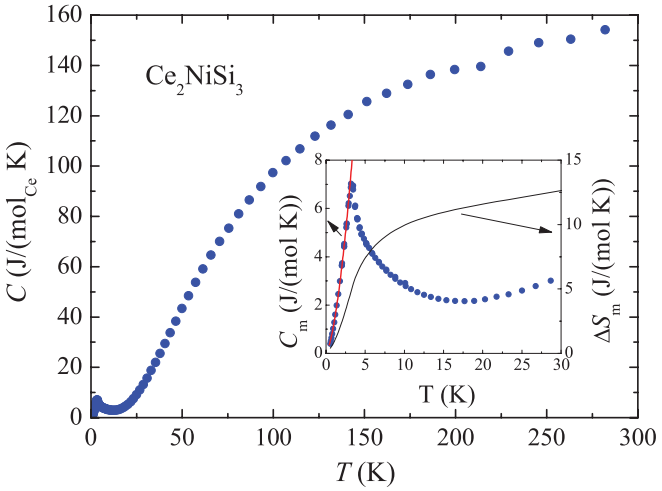

FIG. 5. (Color online) Temperature dependence of the specific heat of single-crystalline Ce_2NiSi_3. The inset shows the low-temperature nonphonon contribution to the heat capacity (left-hand-side axis) and the related magnetic entropy (right-hand-side axis). The solid line represents the least-squares fit described in the text.

a pronounced λ-like anomaly at 3.2 K, which manifests the antiferromagnetic phase transition. A fairly extended tail of this peak above the Néel temperature may be attributed to short-range magnetic correlations. As shown in Fig. 6, application of the magnetic field $B \geqslant 1.5$ T, oriented perpendicular to the hexagonal c axis, brings about considerable broadening of the specific-heat maximum that gradually moves toward higher temperatures with increasing of the field strength. Such behavior, typical of ferromagnets and field-induced ferromagnetic systems, remains in full accord with the scenario of metamagnetic transition occurring in Ce_2NiSi_3 at a field lower that 0.7 T.

Assuming that the phonon contribution to the specific heat of Ce_2NiSi_3 may be well approximated by that of La_2NiSi_3,

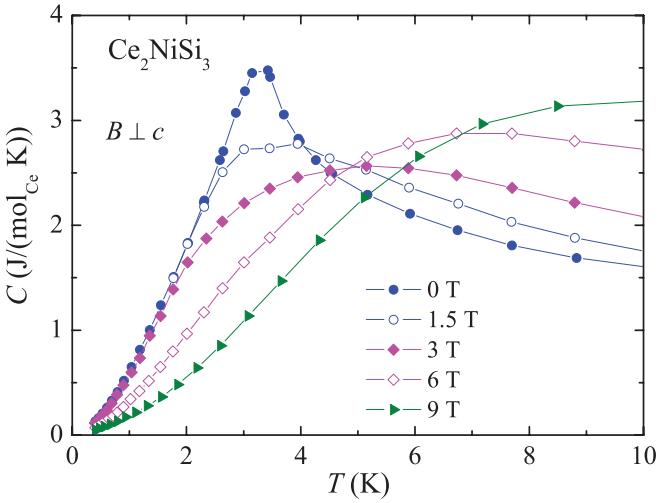

FIG. 6. (Color online) Low-temperature variations of the specific heat of single-crystalline Ce_2NiSi_3 measured in a few different magnetic fields oriented perpendicular to the hexagonal c axis. The thin solid lines serve as a guide for the eye.

the specific heat due to $4f$ electrons was extracted as follows:

$$C_m(T) = C(Ce_2NiSi_3) - C(La_2NiSi_3). \quad (1)$$

As demonstrated in the inset to Fig. 5, in the ordered region, the magnetic contribution to the specific heat of Ce_2NiSi_3 can be well described by the formula[29,30]

$$C_m = \gamma T + c\Delta_{SW}^{7/2}\sqrt{T}\exp\left(\frac{-\Delta_{SW}}{T}\right) \times\left[1+\frac{39\,T}{20\,\Delta_{SW}}+\frac{51}{32}\left(\frac{T}{\Delta_{SW}}\right)^2\right], \quad (2)$$

which accounts for the contributions due to heavy electrons (the first term) and due to antiferromagnetic spin waves (the second term). The applied model assumes the magnon dispersion of the form $\omega = \sqrt{\Delta_{SW}^2 + Dk^2}$, where Δ_{SW} is a gap in the spin-wave spectrum and D stands for the spin-wave stiffness that defines the coefficient $c \propto D^{-3}$ in Eq. (2). The least-square-fitting procedure yielded the parameters $\gamma = 400$ mJ mol_{Ce}^{-1} K^{-2}, $c = 95$ mJ mol_{Ce}^{-1} K^{-4}, and $\Delta_{SW} = 1.5$ K. Apparently, the electronic contribution to the specific heat is strongly enhanced, which implies strong electronic correlations. The spin-wave gap Δ_{SW} is of the order of magnitude often found in Ce-based intermetallics with antiferromagnetic ground states.[31,32]

The Kondo interactions in antiferromagnetic systems usually manifest themselves in some reduction of the specific-heat jump δC at T_N compared to the value predicted within the mean-field approximation. In the framework of the $S = 1/2$ resonant model, δC is related to the characteristic Kondo temperature T_K via the formula[33,34]

$$\delta C = \frac{6k_B}{\psi'''\left(\frac{1}{2}+\zeta\right)}\left[\psi'\left(\frac{1}{2}+\zeta\right)+\zeta\psi''\left(\frac{1}{2}+\zeta\right)\right]^2, \quad (3)$$

where $\zeta = (T_K/T_N)/2\pi$, while ψ', ψ'', and ψ''' are first three derivatives of the digamma function. This universal relation is presented in Fig. 7. For Ce_2NiSi_3 the value of δC is about 2.13 J mol_{Ce}^{-1} K^{-1}, which yields T_K equal to about 8 K.

Another estimation of T_K can be derived from the magnetic entropy released by the antiferromagnetic phase transition,

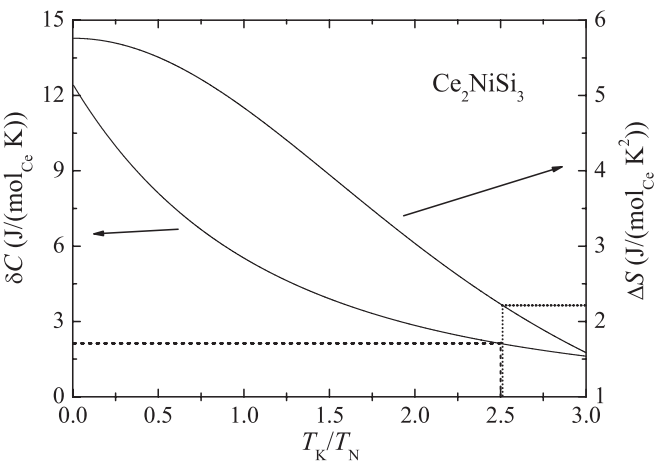

FIG. 7. Illustration of the methods used for estimating the Kondo temperature in Ce_2NiSi_3 (see the text).

which is given by the equation[35]

$$\Delta S(T_N) = \mathrm{R}\left\{\ln\left[1+\exp\left(\frac{-\mathrm{T_K}}{\mathrm{T_N}}\right)\right]\frac{\mathrm{T_K}}{\mathrm{T_N}}\frac{\exp\left(\frac{-\mathrm{T_K}}{\mathrm{T_N}}\right)}{1+\exp\left(\frac{-\mathrm{T_K}}{\mathrm{T_N}}\right)}\right\}. \quad (4)$$

For Ce_2NiSi_3 the entropy measured at T_N amounts to 2.2 J mol_{Ce}^{-1} K^{-2} (see the inset of Fig. 5), which implies the Kondo temperature of about 8 K (see Fig. 7), in very good agreement with the value estimated from δC.

The above estimation was made on the assumption that all of the reduction of the magnetic entropy released by the Néel temperature results solely from the Kondo interactions. However, one should take into account that in crystallographically disordered compounds, such as Ce_2NiSi_3, some of the entropy freezing may be due to short-range magnetic correlations. As can be inferred from the inset of Fig. 5, the extended tail in $C_m(T)$ indeed contains some notable amount of the entropy. For this reason, the derived value of T_K should be treated as a rough estimate for the upper limit of the actual magnitude of the Kondo temperature in the compound studied.

D. Electrical resistivity

The temperature dependencies of the electrical resistivity of Ce_2NiSi_3, measured with the current flowing perpendicular and parallel to the c axis of the hexagonal unit cell, are presented in Fig. 8. The values of the resistivity for both directions are large and do not change significantly in the entire temperature range studied. This feature probably results from the inherent crystallographic disorder in the AlB_2-type unit cell. The resistivity taken within the a-b plane, $\rho^{\perp}$, amounts to 380 $\mu\Omega$ cm at room temperature and continuously decreases to 315 $\mu\Omega$ cm at 0.4 K. In turn, the resistivity measured along the c axis, $\rho^{\parallel}$, is equal to 290 $\mu\Omega$ cm at 300 K, decreases with decreasing temperature down to about 60 K, and then starts to increase. At lower temperatures, $\rho^{\parallel}(T)$ shows a maximum at 6 K and finally drops down to a value of 283 $\mu\Omega$ cm at

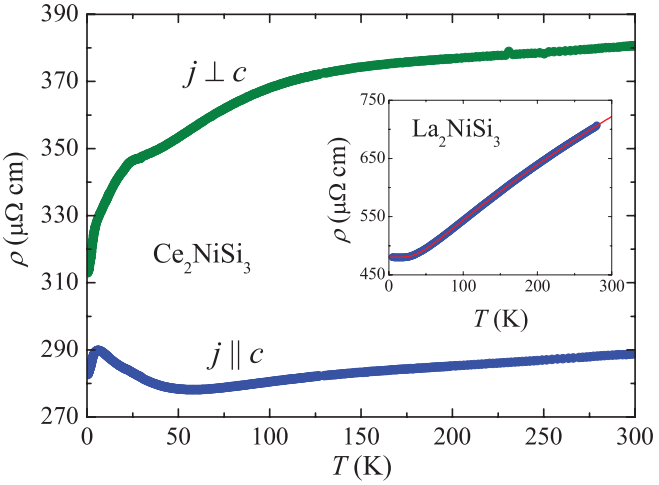

FIG. 8. (Color online) Temperature dependencies of the electrical resistivity of single-crystalline Ce_2NiSi_3 measured with the current flowing along two characteristic directions. The inset presents resistivity data of La_2NiSi_3. The solid line is a BGM fit, described in the text.

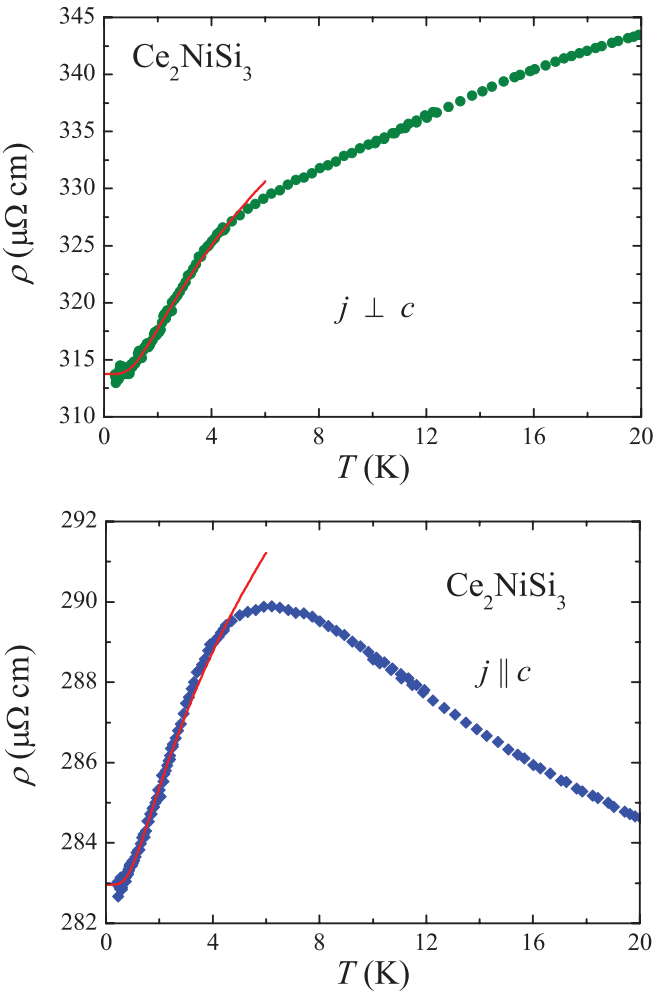

FIG. 9. (Color online) Low-temperature variations of the electrical resistivity of single-crystalline Ce_2NiSi_3 measured with the current flowing perpendicular (upper panel) and parallel (lower panel) to the crystallographic c axis. The solid lines represent the magnon contribution described in the text.

0.4 K. For both current directions a faint hump of unclear origin occurs on the resistivity curve near 25 K.

Below the Néel temperature the resistivity decreases due to reduced scattering of the conduction electrons on disordered magnetic moments. For both resistivity components, the magnetic phase transition manifests itself as an inflection point, well seen on the low-temperature dependencies $\rho^{\perp}(T)$ and $\rho^{\parallel}(T)$, shown in Fig. 9. In the ordered region, the resistivity of Ce_2NiSi_3 can be described by the equation[30,36]

$$\rho(T) = \rho_0 + b\Delta_{\mathrm{SW}}^2\sqrt{\frac{T}{\Delta_{\mathrm{SW}}}}\exp\left(\frac{-\Delta_{\mathrm{SW}}}{T}\right) \times\left[1+\frac{2\,\Delta_{\mathrm{SW}}}{3\,T}+\frac{2}{15}\left(\frac{\Delta_{\mathrm{SW}}}{T}\right)^2\right], \quad (5)$$

which takes into account scattering processes of conduction electrons on lattice defects (the first term) and on antiferromagnetic spin waves with the gap Δ_{SW} in their spectrum (the second term); scattering on phonons was neglected because of the very low temperatures considered. In the above expression, the coefficient b is related to the spin-wave stiffness D as

$b \sim D^{-3/2}$, and the magnon dispersion was assumed to be $\omega = \sqrt{\Delta_{SW}^2 + Dk^2}$, as in the analysis of the specific heat. Least-squares fitting of Eq. (5) to the experimental data yielded the parameters $\rho_0 = 314\ \mu\Omega$ cm, $\Delta_{SW} = 4$ K, $b = 1.1\ \mu\Omega\,\mathrm{cm\,K^{-2}}$ for $j \perp c$ and $\rho_0 = 283\ \mu\Omega$ cm, $\Delta_{SW} = 3.5$ K, and $b = 0.7\ \mu\Omega\ \mathrm{cm\ K^{-2}}$ for $j \parallel c$. The so-obtained values of the spin-wave gap are somewhat larger than that estimated from the heat-capacity data, yet are reasonably close to it.

The inset of Fig. 8 presents the temperature dependence of the electrical resistivity of polycrystalline La_2NiSi_3. The $\rho(T)$ curve of this nonmagnetic counterpart to Ce_2NiSi_3 can be approximated by the function

$$\rho(T) = \rho_0 + \rho_{BGM}(T), \tag{6}$$

where ρ_0 is the residual resistivity due to defects and ρ_{BGM} stands for the Bloch-Grüneisen-Mott contribution, expressed by the equation

$$\rho_{BGM}(T) = 4R\Theta_R \left(\frac{T}{\Theta_R}\right)^5 \int_0^{\Theta_R/T} \frac{x^5 dx}{(e^x - 1)(1 - e^{-x})} - \mathrm{KT}^3, \tag{7}$$

in which the first term accounts for electron-phonon interactions (Θ_R can be considered as an approximation of the Debye temperature) and the second one describes the s-d interband scattering. The least-square fitting of the above equations to the experimental data gave the following parameters: $\rho_0 = 480\ \mu\Omega$ cm, $\Theta_R = 248$ K, $R = 0.89\ \mu\Omega$ cm K^{-1}, and $K = 5.4 \times 10^{-7}\ \mu\Omega$ cm K^{-3}. Similarly to the case of Ce_2NiSi_3, the very large magnitude of the residual resistivity of the La-based compound can be rationalized in terms of the atomic disorder in the crystallographic unit cell.

Assuming that the phonon contribution to the electrical resistivity of Ce_2NiSi_3 is similar to that in the isostructural La-based counterpart, the magnetic resistivity component due to the presence of $4f$ electrons can be estimated as

$$\rho_{mag}(T) + \rho_0 = \rho(T) - \rho_{BGM}(T). \tag{8}$$

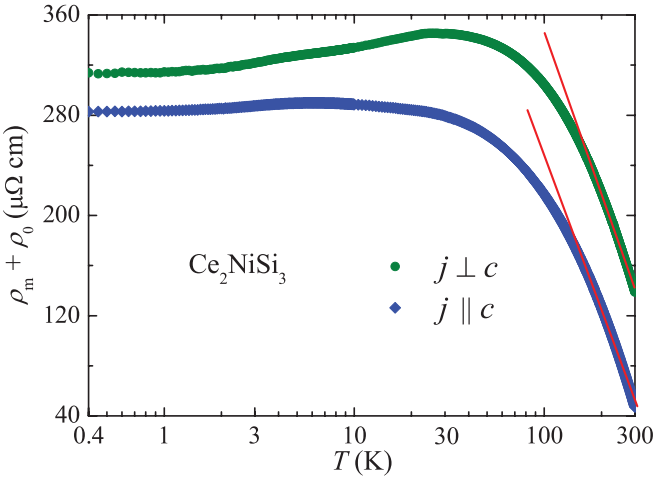

FIG. 10. (Color online) Magnetic contribution to the resistivity of single-crystalline Ce_2NiSi_3 for the current flowing along two characteristic directions (note the semilogarithmic scale). The solid straight lines emphasize the Kondo behavior in the paramagnetic state.

The so-derived $\rho_{mag}^{\perp}(T)$ and $\rho_{mag}^{\parallel}(T)$ variations are displayed in Fig. 10. In the paramagnetic region, both components show similar negative logarithmic slopes, characteristic of Kondo compounds.

E. Magnetoresistivity

Figure 11(a) presents the low-temperature dependencies of the electrical resistivity taken along the c direction, in various magnetic fields oriented within the a-b plane. With raising of the field strength the resistivity gradually decreases, and the maximum on $\rho^{\parallel}(T)$ shifts toward higher temperatures. The transverse magnetoresistivity, defined as $\mathrm{MR} = \frac{\rho(B)-\rho(0)}{\rho(0)}$, measured for the same directions of the current and magnetic field, is shown in Fig. 11(b) as a function of B. In the ordered region, the MR curves exhibit small positive maxima in weak fields (MR $\approx 0.2\%$ at 1 K in a field of 0.5 T). This behavior is typical of antiferromagnets undergoing field-induced metamagnetic transition, and the position of the MR maximum coincides with the critical field estimated from the magnetic

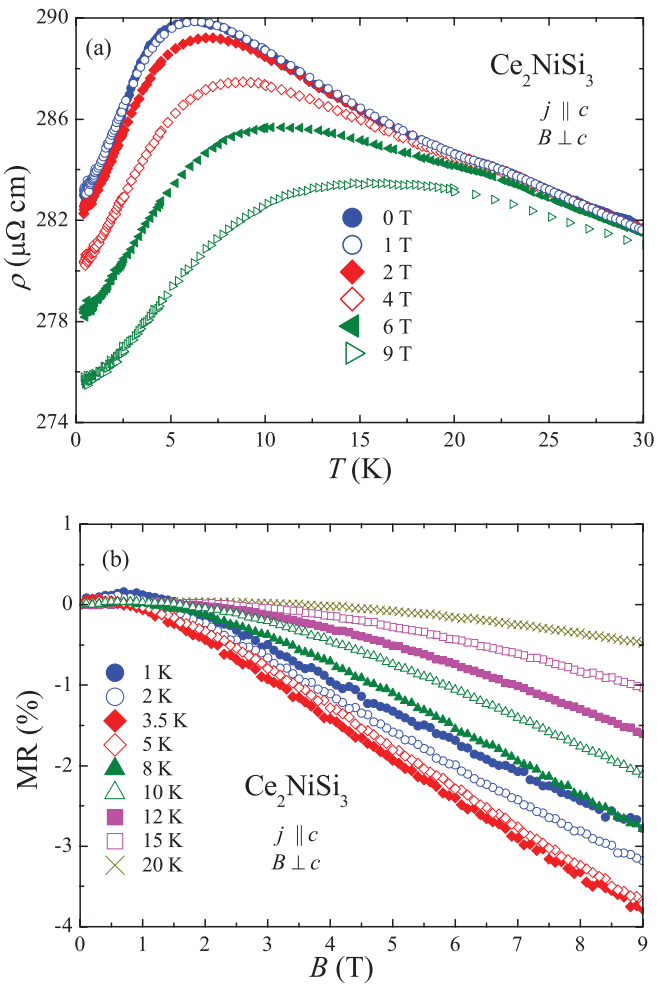

FIG. 11. (Color online) (a) Low-temperature variations of the electrical resistivity of single-crystalline Ce_2NiSi_3 measured along the c axis in different magnetic fields applied within the a-b plane. (b) Transverse magnetoresistivity isotherms of Ce_2NiSi_3 taken at several temperatures from the ordered and paramagnetic regions with the configurations of the electrical current and the magnetic field as in panel (a).

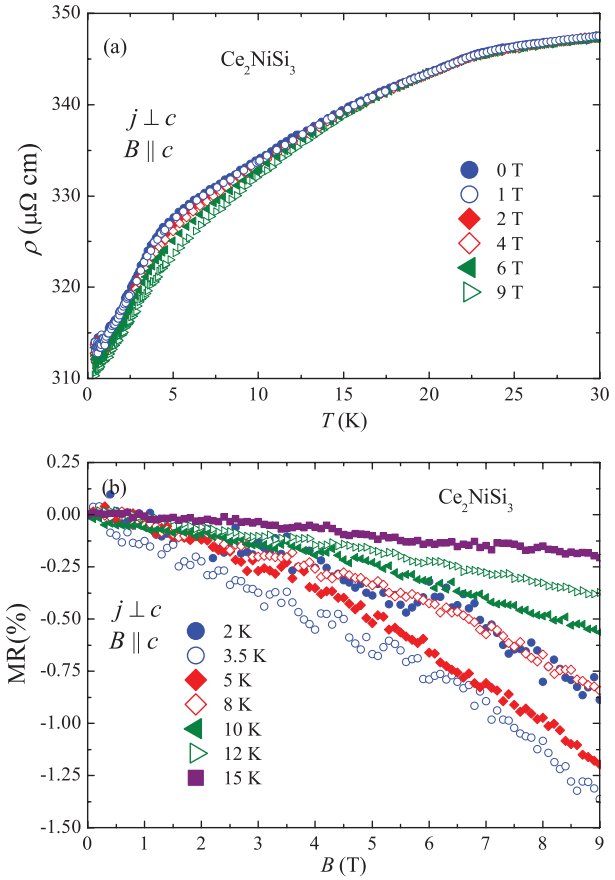

FIG. 12. (Color online) (a) Low-temperature variations of the electrical resistivity of single-crystalline Ce_2NiSi_3 measured with the current flowing within the a-b plane in different magnetic fields applied along the c axis. (b) Transverse magnetoresistivity isotherms of Ce_2NiSi_3 taken at several temperatures from the ordered and paramagnetic regions with the configurations of the electrical current and the magnetic field as in panel (a).

susceptibility data. In stronger fields, the transverse magnetoresistivity is negative and its absolute values increase with increasing field, reaching a value of about -3% in 9 T at $T = 2$ K.

The influence of the magnetic field applied along the c axis on the resistivity taken within the a-b plane (see Fig. 12) is much smaller than that for the other field and current configuration. The magnitude of $\rho^{\perp}$ at low temperatures decreases only slightly, and the hump at 5 K somewhat flattens. The transverse magnetoresistivity in the ordered region does not exceed -1%.

In the paramagnetic region, the transverse magnetoresistivity of Ce_2NiSi_3 is negative for both directions of the flowing current and applied magnetic field and varies in a manner characteristic of Kondo systems [see Figs. 11(b) and 12(b)]. MR shows rather moderate anisotropy: while in a field of 9 T, MR taken with $j \parallel c$ and $B \perp c$ reaches a value of about -4% just above T_N, and MR measured with $j \perp c$ and $B \parallel c$ is three times smaller at this temperature.

IV. SUMMARY

Ce_2NiSi_3 crystallizes with the hexagonal AlB_2-type crystal structure with inherent disorder between the Ni and Si atoms, which share the same position in the crystallographic unit cell. Nevertheless, at odds with a simplistic anticipation for the R_2TM_3 phases, the compound orders antiferromagnetically at $T_N = 3.2$ K. The onset of the long-range ordering gives rise to distinct anomalies in the temperature dependencies of the magnetic susceptibility, the heat capacity, and the electrical resistivity. In the ordered state, the specific heat and the electrical resistivity are dominated by the contributions due to antiferromagnetic magnons. The bulk magnetic data hint at an antiferromagnetic structure with the cerium magnetic moments confined in the hexagonal a-b plane. They also indicate the presence of a small ferromagnetic component. This magnetic structure appears very sensitive to external magnetic fields; namely, a field as small as about 0.5 T, oriented perpendicular to the c axis, is able to induce a ferromagneticlike alignment of the magnetic moments. In order to determine the actual magnetic structure of Ce_2NiSi_3, a neutron-diffraction experiment is indispensable.

Large negative values of the paramagnetic Curie temperature ($|\theta_P| \gg T_N$), logarithmic temperature variations of the magnetic contribution to the electrical resistivity, the characteristic shape of the negative transverse magnetoresistivity curves, as well as the strongly enhanced value of the low-temperature specific heat, reduced specific-heat jump at the antiferromagnetic phase transition, and fairly small magnetic entropy released by the Néel temperature—all these features of Ce_2NiSi_3 unanimously signal a substantial role played by the Kondo interactions with the characteristic energy scale of about 8 K.

In this respect, the present compound closely resembles the antiferromagnetic Kondo lattices Ce_2RhSi_3[32] and Ce_2IrSi_3,[37] which crystallize, however, in a fully ordered derivative of the AlB_2-type structure. On the other hand, Kondo screening interactions have been evidenced also in Ce_2NiGe_3[23] and Ce_2NiIn_3,[24] which are isostructural with Ce_2NiSi_3 yet do not order magnetically but exhibit instead a spin-glass freezing effect.

ACKNOWLEDGMENTS

The authors are grateful to J. Stepień-Damm and W. Walerczyk for performing the x-ray-diffraction experiments. This work was supported by the Ministry of Science and Higher Education within research Project No. IP 2011 054471.

[1] R.-D. Hoffmann and R. Pöttgen, Z. Kristallogr. **216**, 127 (2001).
[2] C. Tien, C. H. Feng, C. S. Wur, and J. J. Lu, Phys. Rev. B **61**, 12151 (2000).
[3] T. Nishioka, Y. Tabata, T. Taniguchi, and Y. Miyako, J. Phys. Soc. Jpn. **69**, 1012 (2000).
[4] D. Kaczorowski and H. Noël, J. Phys.: Condens. Matter **5**, 9185 (1993).

[5]B. Chevalier, R. Pöttgen, B. Darriet, P. Gravereau, and J. Etourneau, J. Alloys Compd. **233**, 150 (1996).
[6]D. X. Li, Y. Shiokawa, Y. Homma, A. Uesawa, A. Dönni, T. Suzuki, Y. Haga, E. Yamamoto, T. Honma, and Y. Ōnuki, Phys. Rev. B **57**, 7434 (1998).
[7]D. Li, A. Kimura, Y. Homma, Y. Shiokawa, A. Uesawa, and T. Suzuki, Solid State Commun. **108**, 863 (1998).
[8]D. Li, A. Dönni, Y. Kimura, Y. Shiokawa, Y. Homma, Y. Haga, E. Yamamoto, T. Honma, and Y. Ōnuki, J. Phys.: Condens. Matter **11**, 8263 (1999).
[9]D. Li, Y. Shiokawa, Y. Haga, E. Yamamoto, and Y. Ōnuki, J. Phys. Soc. Jpn. **71**, 418 (2002).
[10]D. X. Li, S. Nimori, Y. Shiokawa, Y. Haga, E. Yamamoto, and Y. Ōnuki, Phys. Rev. B **68**, 172405 (2003).
[11]M. Szlawska, D. Kaczorowski, and M. Reehuis, Phys. Rev. B **81**, 094423 (2010).
[12]D. X. Li, A. Kimura, Y. Haga, S. Nimori, and T. Shikama, J. Phys.: Condens. Matter **23**, 076003 (2011).
[13]B. Chevalier, P. Lejay, J. Etourneau, and P. Hagenmuller, Solid State Comm. **49**, 753 (1984).
[14]A. Szytuła, J. Leciejewicz, and K. Małetka, J. Magn. Magn. Mater. **118**, 302 (1993).
[15]I. Das and E. V. Sampathkumaran, J. Magn. Magn. Mater. **137**, L239 (1994).
[16]J. Leciejewicz, N. Stüsser, A. Szytuła, and A. Zygmunt, J. Magn. Magn. Mater. **147**, 45 (1995).
[17]W. Bażela, E. Wawrzyńska, B. Penc, N. Stüsser, A. Szytuła, and A. Zygmunt, J. Alloys Compd. **360**, 76 (2003).
[18]R. A. Gordon, C. J. Warren, M. G. Alexander, F. J. DiSalvo, and R. Pöttgen, J. Alloys Compd. **248**, 24 (1997).
[19]S. Majumdar, M. M. Kumar, R. Mallik, and E. V. Sampathkumaran, Solid State Commun. **110**, 509 (1999).
[20]S. Majumdar and E. V. Sampathkumaran, Phys. Rev. B **62**, 8959 (2000).
[21]T. Yamamura, D. Li, K. Yubuta, and Y. Shiokawa, J. Alloys Compd. **408–412**, 1324 (2006).
[22]O. I. Bodak, M. G. Mis'kiv, A. T. Tyvanchuk, O. I. Kharchenko, and E. I. Gladyshevskii, Izv. Akad. Nauk SSSR, Neorg. Mater. **9**, 864 (1973).
[23]D. Huo, J. Sakurai, T. Kuwai, Y. Isikawa, and Q. Lu, Phys. Rev. B **64**, 224405 (2001).
[24]D. P. Rojas, L. C. J. Pereira, E. B. Lopes, J. C. Waerenborgh, L. M. da Silva, F. G. Gandra, and A. N. Medina, J. Alloys Compd. **432**, 34 (2007).
[25]S. K. Dhar, R. Balasubramanium, S. M. Pattalwar, and R. Vijayaraghavan, J. Alloys Compd. **210**, 339 (1994).
[26]D. P. Rojas, J. Rodríguez Fernández, J. I. Espeso, J. C. Gómez Sal, J. C. da Silva, F. G. Gandra, A. O. dos Santos, and A. N. Medina, J. Magn. Magn. Mater. **322**, 3192 (2010).
[27]G. M. Sheldrick, Acta Crystallographica A **64**, 112 (2008).
[28]J. Rodriguez-Carvajal, Physica B **192**, 55 (1992).
[29]S. N. de Medeiros, M. A. Continentino,, M. T. D. Orlando, M. B. Fontes, E. M. Baggio-Saitovitch, A. Rosch, and A. Eichler, Physica B **281–282**, 340 (2000).
[30]M. A. Continentino, S. N. de Medeiros, M. T. D. Orlando, M. B. Fontes, and E. M. Baggio-Saitovitch, Phys. Rev. B **64**, 012404 (2001).
[31]A. P. Pikul, D. Kaczorowski, T. Plackowski, A. Czopnik, H. Michor, E. Bauer, G. Hilscher, P. Rogl, and Y. Grin, Phys. Rev. B **67**, 224417 (2003).
[32]M. Szlawska, D. Kaczorowski, A. Ślebarski, L. Gulay, and J. Stepień-Damm, Phys. Rev. B **79**, 134435 (2009).
[33]C. D. Bredl, F. Steglich, and K. D. Schotte, Z. Phys. B **29**, 327 (1978).
[34]J. A. Blanco, M. de Podesta, J. I. Espeso, J. C. Gómez Sal, C. Lester, K. A. McEwen, N. Patrikios, and J. Rodríguez Fernández, Phys. Rev. B **49**, 15126 (1994).
[35]H. Yashima, H. Mori, N. Sato, and T. Satoh, J. Magn. Magn. Mater. **31–34**, 411 (1983).
[36]M. B. Fontes, J. C. Trochez, B. Giordanengo, S. L. Bud'ko, D. R. Sanchez, E. M. Baggio-Saitovitch, and M. A. Continentino, Phys. Rev. B **60**, 6781 (1999).
[37]M. Szlawska and D. Kaczorowski, Phys. Rev. B **84**, 094430 (2011).